

Chapter 5

Nonlinear and Tunable Left-Handed Transmission Lines

Alexander B. Kozyrev and Daniel W. van der Weide

5.1 Introduction

Metamaterials are artificial structures that are designed to exhibit specific electromagnetic properties required for different applications but not commonly found in nature. The methodology of synthesizing materials composed of micro- and nano-structured components that mimic the electromagnetic response of individual atoms and molecules (meta-atoms and meta-molecules) has proven to be very productive and resulted in the development of metamaterials exhibiting strong magnetic response at microwave and optical frequencies and so-called left-handed metamaterials (LHMs) (both impossible in conventional real-world materials).

LHMs are designed to exhibit simultaneously negative permittivity and permeability [1, 2]. In 2000, Smith et al. developed the first experimental left-handed (LH) structure, which was composed of metallic split-ring resonators and thin metal wires [3, 4]. An alternative transmission line approach for left-handed materials was proposed, almost simultaneously, by several different groups [5–7]. This approach, based on nonresonant components, allows for low-loss left-handed structures with broad bandwidth. The unique electrodynamic properties of these materials, first postulated by Veselago in 1968, include the reversal of Snell's law, the Doppler effect, Vavilov-Cherenkov radiation, and negative refractive index, making these materials attractive for new types of RF and microwave components [1, 2, 8]. The range of applications for LHMs is extensive, and opportunities abound for development of new and powerful imaging and communication techniques.

Most studies of LHMs have been concerned with linear wave propagation, and have inspired many applications that were unthinkable in the past [1, 9] such as LH phase shifters [10], LH directional couplers [11, 12], and leaky-wave antennas

A.B. Kozyrev (✉) · D.W. van der Weide
Department of Electrical and Computer Engineering, University of Wisconsin-Madison,
Madison, WI 53706, USA
e-mail: alexander.kozyrev@gmail.com

[13–15] to name just a few. Materials that combine *nonlinearity* with the anomalous dispersion exhibited by LH media [16–19], however, give rise to a new class of phenomena and promising applications [20–22]. Here we present a review of the basic *nonlinear* wave propagation phenomena in LH media. We consider left-handed nonlinear transmission lines (LH NLTL) as the simplest systems that would allow us to combine anomalous dispersion with nonlinearity in a controlled fashion. Understanding the nonlinear phenomena in LH NLTL media is important for both the development of new devices and improvement of the performance of recent devices based on LH NLTLs like harmonic generators, phase shifters [23], tunable leaky-wave antennas [9, 24] and notch filters [25].

5.2 Comparison of Conventional Right-Handed and Left-Handed Nonlinear Transmission Lines

The transmission line approach proves to be a useful description of LH media. It provides insight into the physical phenomena of LH media and is an efficient design tool for LH applications [9]. A LH NLTL is the dual of a conventional right-handed nonlinear transmission line (RH NLTL) shown in Fig. 5.1b, where inductors are replaced with capacitors and capacitors with inductors. The effective permeability and permittivity of one-dimensional transmission line metamaterials in the lossless case are expressed as follows:

$$\mu_{eff} = -\frac{2d}{\omega^2 C_L}; \quad \varepsilon_{eff} = -\frac{d}{\omega^2 L_L}, \quad (5.1)$$

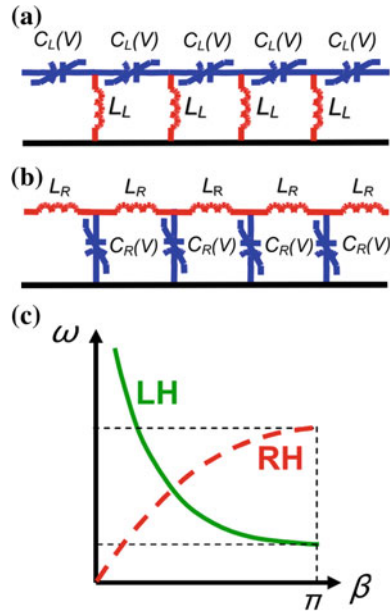
where d is the period of the LH NLTL and ω is the radian frequency. In contrast with RH NLTL where capacitance gives rise to electric nonlinearity, nonlinear capacitances C_L introduce magnetic-type nonlinearity into the LH NLTL (i.e. effective magnetic permeability becomes nonlinear).

Although both the RH and LH NLTLs use the same components arranged in a similar way, the performance of this two circuits is dramatically different. This difference primarily comes from the difference in their dispersion characteristics (see Fig. 5.1c).

A conventional (right-handed) nonlinear transmission line has normal dispersion and frequency increases with the wavenumber. In contrast to the RH NLTL, the LH transmission line exhibits anomalous dispersion and frequency decreases with the wave number (see Fig. 5.1c). The waves propagating in such media are also known as backward waves because the direction of group velocity v_g is opposite to phase velocity ($v_p \cdot v_g < 0$).

Nonlinear transmission lines first drew attention in connection with the idea of distributed parametric amplification. It had been predicted that a distributed parametric amplifier or oscillator circuit could exhibit superior stability of operation and efficiency over lumped parametric circuits [26, 27]. Lumped parametric amplifiers

Fig. 5.1 **a** Equivalent circuit of a LH NLTL; **b** Equivalent circuit of a dual RH NLTL; **c** Typical dispersion curves of LH NLTL (*solid line*) and RH NLTL (*dashed line*)



were popular as very low-noise alternatives to vacuum tubes prior to the widespread use of semiconductor amplifiers [28]. (Parametric resonance responsible for amplification in lumped circuits is similar to the physical mechanism playing on a swing which allows large amplitudes by alternately raising and lowering the center of mass at a certain relation between the frequency of the swing and the frequency of external force.) Their complexity (they require external resonators and matching circuits) and low efficiencies however made them less attractive for widespread use. Conventional NLTLs were thought to be very promising candidates for use in distributed amplifiers because they do not require external resonant circuits and conversion efficiency was claimed to be very high due to accumulative effect of parametrically interacting waves propagating along NLTLs.

It turned out that parametric interactions (such as three- and four-wave mixing of phase matched waves) in RH NLTLs typically compete with shock wave formation [29, 30] and generation of temporal solitons [31]. For instance, parametric generation and amplification in dispersionless RH transmission lines is entirely suppressed by shock wave formation [32, 33]. In contrast to conventional NLTLs, both nonlinearity and dispersion present in LH NLTLs (see Fig. 5.1) lead to waveform spreading [34], consequently making shock wave and electronic soliton formation impossible. Anomalous dispersion makes sharp field transients in left-handed NLTL unstable. Once created, they decompose very quickly during propagation of the waveform due to substantial difference in the phase velocities of the propagating waves. This inability to form shock waves enables a variety of parametric processes to occur

instead [35, 36]. Furthermore, since the parametric interactions no longer compete with shock wave formation, it is possible to use stronger nonlinearities, consequently achieving considerable gain in shorter transmission lines [37].

Both theoretical [36, 38] and experimental [35, 37] investigations demonstrate that nonlinear wave form evolution in a LH NLTL can be understood in terms of competition between harmonic generation, subharmonic generation, frequency down conversion and parametric instabilities.

5.3 Parametric Generation and Amplification

5.3.1 Theory

Effective parametric interaction in medium exhibiting a second-order nonlinearity generally requires phase matching of three waves. The anomalous dispersion of a LH NLTL system enables effective parametric interactions of the type:

$$f_1 + f_2 = f_3, \quad \beta_1 - \beta_2 = \beta_3. \quad (5.2)$$

In the “parametric oscillator configuration”, a high-frequency backward pump wave having a frequency f_3 and wavenumber β_3 is excited by the voltage source connected at the input port of a LH NLTL. It generates two other waves having frequencies f_1 and f_2 , such that $f_1 < f_2$ and $f_1 + f_2 = f_3$. The wave having frequency f_2 propagates in the opposite direction relative to the pump wave and the wave having frequency f_1 (this is emphasized in the (5.2) with the minus sign). We therefore have a similar situation to backward wave parametric generation [38, 39]. The backward-propagating parametrically generated wave f_2 enables internal feedback that results in a considerable energy transfer from the pump wave to the parametrically excited waves.

If the amplitude of a high-frequency pump wave exceeds a certain threshold value, it may parametrically generate two other waves. This threshold value depends on the loss present in the LH NLTL, its length and the boundary conditions (matching) at the input and output. No parametric generation occurs when the amplitude of the voltage source is below this value. However, when a weak signal wave is fed into the LH NLTL together with a pump wave having an amplitude below the threshold value, a parametric amplification is observed. In this case, we have two input waves: an intense pump wave and a weak signal wave [40]. The power from the pump wave is transferred to the signal wave, thus amplifying it. A third parasitic idler wave is generated which provides phase matching. From a previous analysis [38], for the lossless case, the frequencies and powers of these waves also obey the nonlinear Manley-Rowe relations.

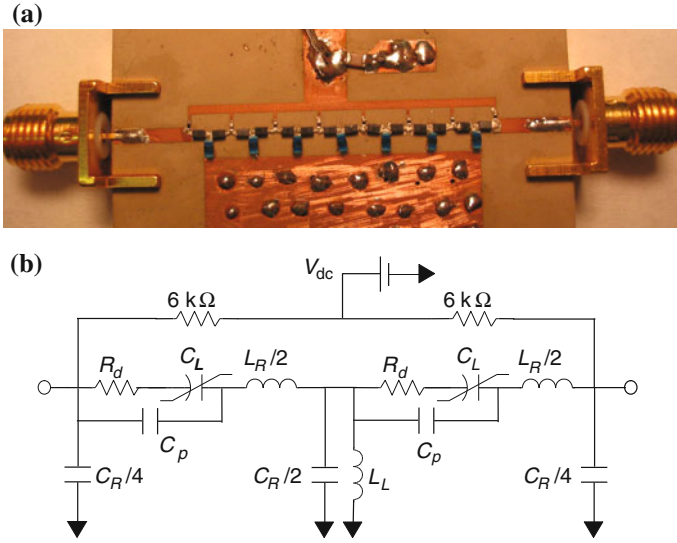
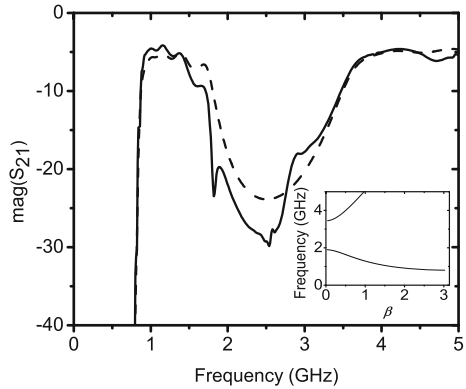


Fig. 5.2 **a** Fabricated 7-section LH NLTL; **b** equivalent circuit of one stage

Fig. 5.3 Measured (*solid*) and simulated (*dashed*) magnitudes of S_{21} parameter for 7-section LH NLTLs for the reverse bias voltage $V_B = 3.823$ V. Inset shows dispersion curve of the LH NLTL (dependence of the frequency versus relative wave number β)



5.3.2 Experiment

We observed efficient parametric amplification in 7-section LH NLTL having identical sections [37] shown in Fig. 5.2a.

The circuit was realized on a Rogers RT/Duroid 3010 board with $\epsilon = 10.2$ and thickness $h = 1.27$ mm. The entire circuit has been implemented using a microstrip geometry. Series nonlinear capacitance in each section is formed by two back-to-back Skyworks Inc. SMV1233 silicon hyperabrupt junction varactors with DC bias applied between them. Shunt inductances were implemented using high-Q 10 nH chip inductors (Murata LQW18A_00). The pads on the board surface, together with

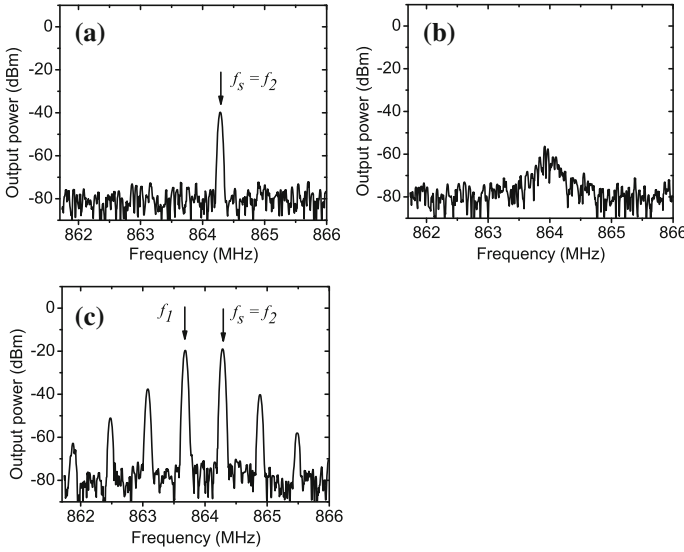


Fig. 5.4 Spectra of the output waveforms generated by a 7-section LH NLTL fed by: **a** only weak signal 864.252 MHz, -28 dBm; **b** only pump source 1.7279 GHz, 13.96 dBm; **c** simultaneously signal and pump sources specified in **a** and **b**. Reverse bias voltage is 3.87 V

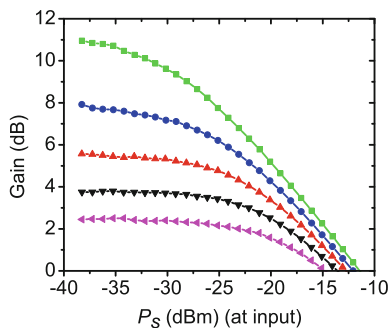
inherent parasitics introduce unavoidable series inductance and shunt capacitance, making the whole circuit a composite right/left-handed transmission line having the equivalent circuit shown in Fig. 5.2b. Figure 5.3 shows measured and simulated magnitude of the linear wave transmission (S_{21}) of this 7-section LH NLTL. The circuit model of Fig. 5.2b with component values extracted from measured S-parameters has also been used to calculate the dispersion curve of the LH transmission line as shown in the inset in Fig. 5.3. The dispersion characteristic of a composite right/left-handed transmission line has two passbands divided by the stop band. The low frequency passband exhibits anomalous dispersion (left-handed passband from 800 MHz to 1.9 GHz) while the high-frequency one is right-handed.

Figure 5.4 demonstrates the effect of the intensive pump wave, having frequency $f_p = f_3$, on a weak signal wave ($f_s = f_2$). Figure 5.4b shows the spectrum at the output of the 7-section LH NLTL when only a 1.7279 GHz, 13.96 dBm intensive pump wave is applied at the input. The magnitude of the pump wave was chosen so as to be 0.1 dB below the threshold value required for the occurrence of parametric generation, which manifests itself in distinct, narrow peaks corresponding to the parametrically generated frequencies.

Figure 5.4a shows the spectrum at the output when only the 864.252 MHz, -28 dBm signal wave is applied at the LH NLTL input (no pump wave). The graph shows 11.7 dB attenuation of the weak signal wave at the output due loss in the NLTL and power conversion to higher harmonics. And finally, Fig. 5.4c shows the spectrum at the output when the signal and the pump wave are both applied concurrently at the

Fig. 5.5 Measured gain versus power of the signal at the input of LH NLTL for different values of the power of the pump wave at the input

$P_{p,in}$: squares –
 $P_{p,in} = 13.96$ dBm; circles –
 $P_{p,in} = 13.86$ dBm;
 up triangles –
 $P_{p,in} = 13.76$ dBm;
 down triangles –
 $P_{p,in} = 13.66$ dBm;
 left triangles –
 $P_{p,in} = 13.56$ dBm



input of the 7-section LH NLTL. In this spectrum, the components corresponding to the signal wave ($f_s = f_2$), idler wave (f_1), as well as many difference frequencies generated due to the strong nonlinearity in LH NLTL, are evident. Thus, the application of the intensive pump wave results in amplification of the weak signal by 9 dB.

Figure 5.5 represents the measured gain of a weak 864.252 MHz signal stimulated by an intense 1.7279 GHz pump wave versus the power of the signal at the input, for fixed values of the pump power. The gain was calculated as the difference between the power of the signal at the output and the power at the input when both are expressed in dBm. Thus, we measured a greater than 10 dB amplification of the signal with power of -32 dBm and below for the power of the pump wave at the input of 13.96 dBm. The measured dependencies of gain versus input signal power becomes flatter with decreasing pump power, thus revealing the potential for amplification in a broad band of the signal power. The results of our measurements in Fig. 5.5 are in a good agreement with the results of simulations reported in [41].

5.3.3 Motivation for Considering Parametric Generation and Amplification

Parametric amplification can be of interest for building “active” or “amplifying” metamaterials and for providing a means to compensate for inherent LH media loss, as suggested in [37, 41, 42]. The primary drawback of current negative-index metamaterials (NIMs) (for example those composed of the arrays of metallic wires and split-ring resonators) is their considerable loss, which renders the results ambiguous and the materials all but useless for practical applications. These losses have been overcome to some extent by careful fabrication and assembly techniques [43], but still remain the primary obstacle to using NIMs in imaging applications. It was shown [44] that due to causality requirements, the use of conventional composite NIMs (based on arrays of metallic wires and arrays of split-ring resonators) does not

allow for the realization of low-loss NIMs without the incorporation of some active components (transistor amplifiers, etc.) in a composite NIM. The idea of using parametric amplification to compensate for inherent loss in optical left-handed systems has been also discussed in [45].

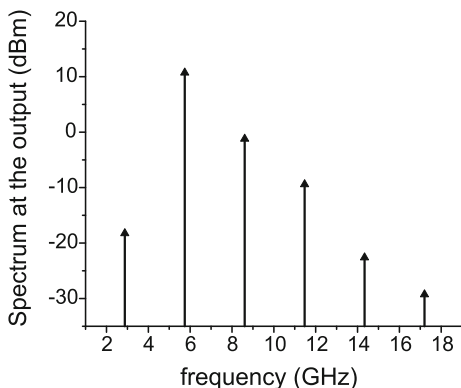
5.4 Higher Harmonic Generation

In short LH NLTLs, harmonic generation dominates over parametric instabilities [36]. We observed very efficient 2nd harmonic generation in a 4-section LH NLTL. The design of this transmission line is similar to the design of 7-section LH NLTL described in the previous section. However, this time, the nonlinear capacitance in each section is formed by two back-to-back M/A-COM hyperabrupt junction GaAs flip-chip varactor diodes (MA46H120) and shunt inductances were implemented with 0.12 mm diameter copper wires connecting the pads to the ground plane on the back side of the board.

The measured value for the second harmonic conversion efficiency in this 4-section LH NLTL was 19% at 2.875 GHz, using a +17.9 dBm input signal and a reverse bias voltage of 6.4 V (Fig. 5.6). The second harmonic power delivered into a 50 Ω load was +10.72 dBm. The fundamental wave is close to the Bragg cutoff frequency while the second harmonic wave is close to the transmission maximum, which is located in the middle of the left-handed passband. A fundamental of 2.875 GHz generates numerous higher harmonics, with the second harmonic dominating over the fundamental and the other harmonics. Thus, the LH NLTL combines the properties of both a harmonic generator and a bandpass filter, and under certain conditions may provide an almost pure higher harmonic at its output.

The conversion efficiency observed in the LH NLTL is comparable with the per-stage efficiency of a hybrid Schottky-diode RH NLTL operated in a lower frequency range [46]. The fundamental wave propagating in the left-handed media is badly mismatched with its higher harmonics due to inherent anomalous dispersion, yet the generation of higher harmonics can still be very effective in LH NLTLs and the discrete nature of the NLTL plays a crucial role in it. The detailed analysis indicates that, within the range of parameters of the pump wave where the 2nd harmonic conversion efficiency has maximum, the amplitude of the voltage oscillations across the nonlinear capacitors varies periodically with the period equal to 2 sections. This self-induced periodicity of the voltage amplitude across the nonlinear capacitors leads to a periodic variation of the capacitance along the line. Due to strong nonlinearity (large capacitance ratio), this periodicity results in a considerable change of the dispersion characteristics and enables quasi-phase matching of the fundamental wave and its second harmonics. Simulations have also shown that, under certain conditions, the self-induced periodicity may provide quasi-phase matching of the fundamental wave with some other higher harmonics in such a way that a particular higher harmonic will dominate over other higher harmonics in the spectrum of the waveform at the LH NLTL output.

Fig. 5.6 Spectrum of the output waveform generated by a π -section LH NLTL fed by 2.875 GHz, +17.9 dBm input signal at reverse bias voltage of 6.4 V



Efficient 2nd harmonic generation can be also achieved in dual band LH NLTLs that allow phase-matching between two zero phase velocity waves, as well as between two backward propagating modes [47].

5.5 Envelope Solitons in LH NLTLs

Besides the nonlinear evolution of a waveform itself, another class of phenomena involving evolution of amplitude and phase of continuous waves is also possible. This type of nonlinear wave propagation phenomena arise in NLTLs having strong frequency dispersion with respect to the average amplitude for amplitude-modulated wave containing a carrier of relatively high frequency. This dispersion may lead to amplitude instability as well as to formation of envelope solitons and periodic modulation of a carrier wave propagating in a stationary manner. The observation of amplitude instability and envelope soliton generation in conventional (RH) NLTLs has already been the subject of many publications [48–50]. The experimental observation of the generation of the trains of envelope solitons in LH NLTLs arising from the self-modulational instability was first reported in [51].

The analysis of LH NLTLs is straightforward when the equations governing envelope evolution can be reduced to the one-dimensional cubic nonlinear Schrödinger equation (NSE), which provides a canonical description for the envelope dynamics of a quasi-monochromatic plane wave (the carrier) propagating in a weakly nonlinear dispersive medium when dissipative processes (including nonlinear damping due to higher harmonic generation and nonlinear wave mixing) are negligible [52, 53]. However, in most of the practical situations the parametric decay instabilities and higher harmonic generation can be very significant [35, 37, 38, 54]. The threshold for parametric generation is known to be very low (lower than in conventional RH NLTLs). In order to realize the scenario described by the NSE, the LH NLTL should be operated below this threshold so that the nonlinearity should be very

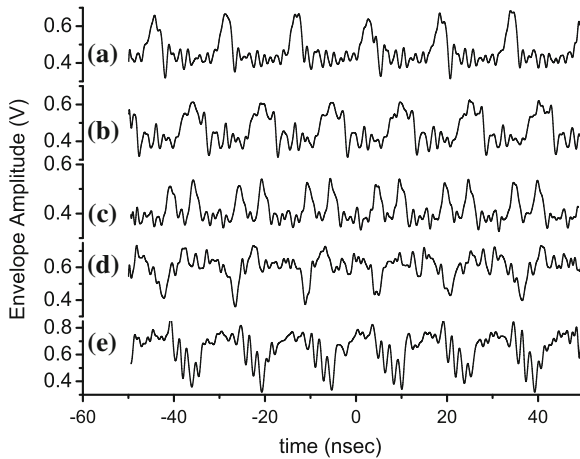


Fig. 5.7 Measured trains of envelope solitons for different power P_{inpp} and the frequency f_{inpp} of the input signal. **a** $f_{inpp} = 1.3723$ GHz, $P_{inpp} = 24.66$ dBm; **b** $f_{inpp} = 1.3125$ GHz, $P_{inpp} = 21.60$ dBm; **c** $f_{inpp} = 1.321596$ GHz, $P_{inpp} = 19.34$ dBm; **d** $f_{inpp} = 1.2974$ GHz, $P_{inpp} = 24.64$ dBm; **e** $f_{inpp} = 1.102$ GHz, $P_{inpp} = 23.62$ dBm

weak and the NLTL impractically long. In contrast, we performed an experimental study of nonlinear envelope evolution and envelope soliton generation in relatively short LH NLTLs and when nonlinear damping is very strong. We are also taking advantage of a fast nonlinearity introduced by Schottky diodes when nonlinear capacitance is a function of the instantaneous value of voltage along the line rather than its amplitude, a type of nonlinearity not described in the framework of the NSE and its modifications developed for slow (retarding) nonlinearity.

Depending on the amplitude and frequency of the input signal, trains of envelope solitons of different shape and types can be generated. Figure 5.7 shows envelopes of the measured waveforms at the output of 7-section LH NLTL. These envelopes' functions have been obtained by applying the Hilbert transform to the original voltage waveforms. Traces (a), (b) and (c) in Fig. 5.7 show trains of bright envelope solitons of different shapes while traces (d) and (e) show periodic trains of dark-like solitons (dips in the cw background). The envelope shape is not smooth since strong nonlinearity gives rise to numerous higher harmonics and subharmonics of carrier frequency. In the spectral domain, generation of envelope solitons manifests itself in the appearance of spectral regions with numerous closely spaced spectral harmonics. The interval between adjacent spectral components is $\Delta f = 1/\tau$, where τ is the period of the train of solitons.

A small variation of the parameters of the input signal leads to switching between the generation of bright and dark solitons [compare traces (a) and (b)] in contrast to the scenario described by the NSE. The observed switching is enabled by the counterplay of the significant nonlinear damping (due to strong and fast nonlinearity) and strong spatial dispersion exhibited by the periodic LH NLTLs. Neither is taken

into account by standard NSE yet both are known to lead to co-existence of bright and dark solitons in other physical systems [54, 55]. For example, somewhat similar processes have recently been observed in the system of an in-plane magnetized single crystal yttrium-iron-garnet (YIG) film in the magnetostatic backward volume wave configuration [55]. In contrast to this work, we applied non-modulated sine wave at the input.

Furthermore, efficient envelope soliton generation has been observed in active resonant rings based on LH NLTLs. Stable regimes corresponding to one, two and three solitons circulating in the ring has been enabled without any special mode selection arrangements and has been explained as the interplay of anomalous dispersion and discreteness resulting in formation of spatially localized structures [56].

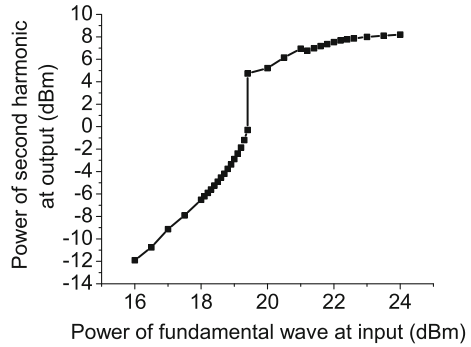
5.6 Pulse Formation in LH NLTL Media

Here we discuss another type of envelope evolution resulting in generation of RF pulses of limited duration with stable amplitude and very short rise/fall times (sharp transients). This type of envelope evolution is primarily enabled by the amplitude-dependent higher harmonic generation rather than self-modulation instability leading to generation of the envelope solitons [57].

Figure 5.8 shows a typical dependence of the magnitude of the second harmonics at the output of 7-section LH NLTL shown in Fig. 5.2 versus magnitude of the input sinusoidal signal. This dependence has three distinct regions. In the first region the power of the generated second harmonic follows a square law as predicted by the small signal analysis. When the power of the fundamental wave reaches certain threshold level the second harmonic power jumps by almost 5 dB indicating a bifurcation (multistability region) followed by the saturation region where second harmonic amplitude changes insignificantly with the input power. Step-like dependence of the second harmonic power indicates a bifurcation-type change in the field distribution along the line and formation of field patterns that change dispersion properties of the line (quasi-phase matching) resulting in significant increase of the generation efficiency.

The step-like dependence of the second harmonic power on the power of the fundamental signal may impact significantly the output waveform if the amplitude in the fundamental wave is modulated around the threshold value. Figure 5.9 shows voltage waveforms at the input and output port and spectrum at the output of 7-section LH NLTL. The voltage waveform at the input is a sinusoidal wave modulated by another sinusoidal signal at 100 MHz. The envelope of the output waveform is dramatically different from the one of the input wave. It represents itself a series of pulses with the shape approaching a rectangular. Furthermore, the carrier frequency of the output signal is the second harmonic of the fundamental signal as revealed by the spectrum presented in Fig. 5.9c. Modulated signal switches second harmonic generation on and off thus enabling generation of a train of RF pulses at the output. Since the fundamental frequency is chosen below the cut-off frequency, it is heavily

Fig. 5.8 Dependence of the power of the 2nd harmonic at the output on the power of the fundamental signal at the input in 7-section LH NLTL shown in Fig. 5.2 and measured at 783 MHz and the reverse bias voltage $V_B = -4.1$ V



attenuated in transmission line and only second harmonic is present at the output. Some asymmetry of the shape of the RF pulses at the output is related to the existence of hysteresis and narrow multistability region. The experimental results presented

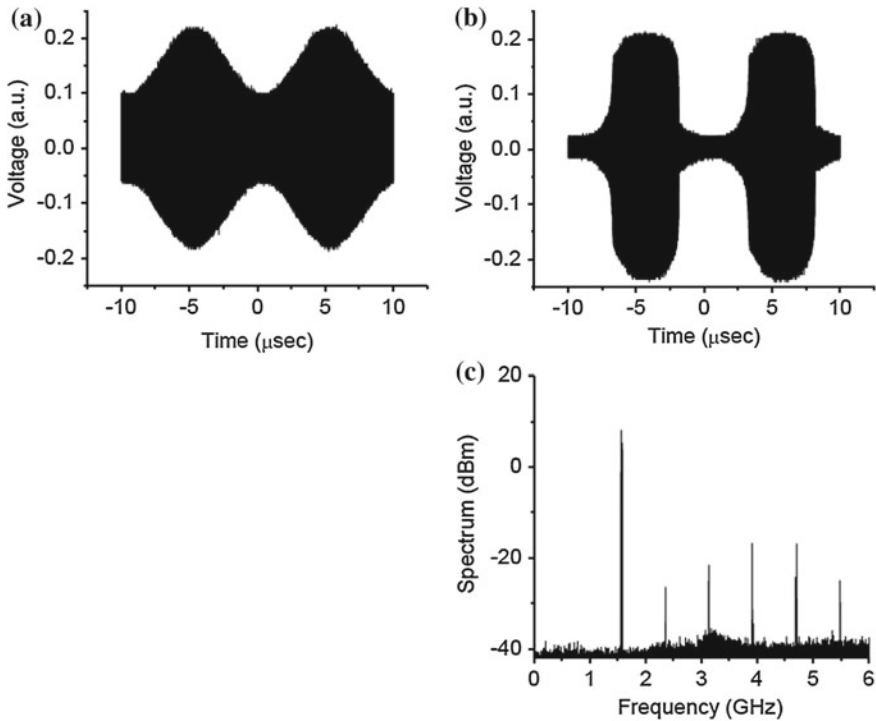


Fig. 5.9 Voltage waveforms at the input (a) and output (b) port and spectrum at the output (c) of 7-section LH NLTL. Voltage was measured at the coupled output of directional couplers connected at the input and output ports of NLTL

in Fig. 5.9 clearly demonstrate that a small modulation signal can be used to control the shape, duration and repetition rate of the RF pulses at the output which is very promising to numerous applications.

Our experimental results correlate very well with speculations in [58] where authors predicted that the shape of pulses at the output of LH media can be drastically different from those expected from an ordinary nonlinear medium.

5.7 Conclusion

We have reviewed several nonlinear wave phenomena in LH NLTL media, including harmonic generation, parametric amplification as well as generation of the trains of envelope solitons and their competition. Furthermore, LH NLTLs which were considered as a model system in this paper, can be also of interest from the design perspective for development of various compact and robust applications for wireless communications and imaging. LH NLTLs have already been used as the key counterparts of recently designed and implemented tunable phase-shifters, tunable band-pass filters, and the arbitrary waveform generator [23, 59–61]. Moreover, extending the results for 1-D LH NLTL to higher dimensions would enable combining harmonic generation in LH NLTL media with focusing [15], due to the negative refractive index of 2-D or 3-D LH transmission line media. This may lead to the development of highly efficient and powerful frequency multipliers, as well as to building “active” or “amplifying” super lenses. Furthermore, our approach can be also scaled from its current microwave form into terahertz, infrared, and, ultimately, visible form [62, 63]. Potential applications may include pulse forming circuits, optical comb generators (in optical metrology systems), amplifiers of digital signals as well as very efficient modulators at power levels or in frequency ranges not attainable by conventional semiconductor devices.

This work was supported under the Air Force Office of Scientific Research, MURI Grant No F49620-03-1-0420, ‘Nanoprobe Tools for Molecular Spectroscopy and Control’.

References

1. N. Engheta, R.W. Ziolkowski, *Metamaterials: Physics and Engineering Explorations* (Wiley, New York, 2006)
2. V.G. Veselago, *Sov. Phys. Uspekhi* **10**, 509 (1968)
3. R.A. Shelby, D.R. Smith, S. Schultz, *Science* **292**, 77 (2001)
4. D.R. Smith, W.J. Padilla, D.C. Vier, S.C. Nemat-Nasser, S. Schultz, *Phys. Rev. Lett.*, **84**, 4184 (2000)
5. A.M. Belyantsev, A.B. Kozyrev, *Tech. Phys.* **47**, 1477 (2002)
6. C. Caloz, T. Itoh, *IEEE Antennas Propag. Soc. Int. Symp. Dig.* **2**, 412 (2002)
7. A.K. Iyer, G.V. Eleftheriades, *IEEE MTT-S Int Symp. Dig.*, **2**, 1067 (2002)

8. J.B. Pendry, Phys. Rev. Lett. **85**, 3966 (2000)
9. A. Lai, C. Caloz, T. Itoh, IEEE Microw. Mag. **5**, 34 (2004)
10. M. Anioniades, G.V. Eleftheriades, IEEE Antenna Wirel. Prop. Lett. **2**, 103 (2003)
11. C. Caloz, A. Sanada, T. Itoh, IEEE Trans. Microw. Theory Tech. **52**, 980 (2004)
12. L. Liu, C. Caloz, C.-C. Chang, T. Itoh, J. Appl. Phys. **92**, 5560 (2002)
13. S. Lim, C. Caloz, T. Itoh, IEEE Trans. Microw. Theory Tech. **53**, 161 (2005)
14. L. Liu, C. Caloz, T. Itoh, Electron. Lett. **38**, 1414 (2002)
15. A. Grbic, G.V. Eleftheriades, J. Appl. Phys. **92**, 5930 (2002)
16. M. Lapine, M. Gorkunov, Phys. Rev. E **70**, 066601 (2004)
17. M. Lapine, M. Gorkunov, K.H. Ringhofer, Phys. Rev. E **67**, 065601 (2003)
18. D.A. Powell, I.V. Shadrivov, Y.S. Kivshar, M.V. Gorkunov, Appl. Phys. Lett. **91**, 144107 (2007)
19. I.V. Shadrivov, S.K. Morrison, Y.S. Kivshar, Opt. Exp. **14**, 20 (2006)
20. A.A. Zharov, I.V. Shadrivov, Y.S. Kivshar, Phys. Rev. Lett. **91**, 037401 (2003)
21. I.V. Shadrivov, Y.S. Kivshar, J., Opt. A Pure Appl. Opt. **7**, 68 (2005)
22. V.M. Shalaev, Nature Photon. **1**, 41 (2007)
23. H. Kim, A.B. Kozyrev, D.W. van der Weide, IEEE Microw. Wirel. Comp. Lett. **15**, 366 (2005)
24. D.F. Sievenpiper, IEEE Trans. Antennas Prop. **53**, 236 (2005)
25. I. Gil, J. Garcia-Garcia, J. Bonache, F. Martin, M. Sorolla, R. Marques, Electron. Lett. **40**, 1347 (2004)
26. A.L. Cullen, Nature **181**, 332 (1958)
27. P.K. Tien, J. Appl. Phys. **29**, 1347 (1958)
28. W.H. Louisell, *Coupled Mode and Parametric Electronics* (Wiley, New York, 1960)
29. A.V. Gaponov, L.A. Ostrovskii, G.I. Freidman, Radiophys. Quant. Electron. **10**, 772 (1967)
30. I.G. Kataev, *Electromagnetic Shock Waves* (Illife, London, 1966)
31. R. Hirota, K. Suzuki, Proc. IEEE **61**, 1483 (1973)
32. R. Landauer, IBM J. **4**, 391 (1960)
33. R. Landauer, J. Appl. Phys. **31**, 479 (1960)
34. C. Caloz, I.H. Lin, T. Itoh, Microw. Opt. Tech. Lett. **40**, 471 (2004)
35. A.B. Kozyrev, H. Kim, A. Karbassi, D.W. van der Weide, Appl. Phys. Lett. **87**, 121109 (2005)
36. A.B. Kozyrev, D.W. van der Weide, IEEE Trans. Microw. Theory Tech. **53**, 238 (2005)
37. A.B. Kozyrev, H. Kim, D.W. van der Weide, Appl. Phys. Lett. **88**, 264101 (2006)
38. A.S. Gorshkov, G.A. Lyakhov, K.I. Voliak, L.A. Yarovoi, Physica D **122**, 161 (1998)
39. S.E. Harris, Appl. Phys. Lett. **9**, 114 (1966)
40. A. Yariv, *Quantum Electronics* (Wiley, New York, 1988)
41. A.B. Kozyrev, D.W. van der Weide, IEEE Antennas Prop. Soc. Int. Symp. Dig. 672 (2005)
42. A.B. Kozyrev, D.W. van der Weide, US Patent 7,135,917 B2 (2006)
43. A.A. Houck, J.B. Brock, I.L. Chuang, Phys. Rev. Lett. **90**, 137401 (2003)
44. S.A. Tretyakov, Microw. Opt. Tech. Lett. **31**, 163 (2001)
45. A.K. Popov, V.M. Shalaev, Opt. Lett. **31**, 2169 (2006)
46. J.-M. Duchamp, P. Ferrari, M. Fernandez, A. Jrad, X. Melique, J. Tao, S. Arscott, D. Lippens, R.G. Harrison, IEEE Trans. Microw. Theory Technol. **51**, 1105 (2003)
47. W.R.C. Somerville, D.A. Powell, I.V. Shadrivov, Appl. Phys. Lett. **98**, 161111 (2011)
48. K.E. Lonngren, A. Scott, *Solitons in Action* (Academic Press, New York, 1978)
49. L.A. Ostrovskii, L.V. Soustov, Izvestiya Vysshikh Uchebnykh Zavedenii. Radiofizika **15**, 242 (1972)
50. T. Yagi, A. Noguchi, Electron. Commun. Japan **59**, 1 (1976)
51. A.B. Kozyrev, D.W. van der Weide, Appl. Phys. Lett. **91**, 254111 (2007)
52. S. Gupta, C. Caloz, IEEE MTT-S Int. Symp. Dig. **18**, 979-982 (2007)
53. K. Narahara, T. Nakamichi, T. Suemitsu, T. Otsuji, E. Sano, J. Appl. Phys. **102**, 024501 (2007)
54. Y.S. Kivshar, W. Krolikowski, O.A. Chubykalo, Phys. Rev. E **50**, 5020-32 (1994)
55. M.M. Scott, M.P. Kostylev, B.A. Kalinikos, C.E. Patton, Phys. Rev. B **71**, 174440 (2005)
56. A.B. Kozyrev, I.V. Shadrivov, Yu.S. Kivshar, Appl. Phys. Lett. **104**, 084105 (2014)
57. A.B. Kozyrev, D.W. van der Weide, Appl. Phys. Lett. **96**, 104106 (2010)
58. V.M. Agranovich, Y.R. Shen, R.H. Baughman, A.A. Zakhidov, Phys. Rev. B **69**, 165112 (2004)

59. H. Kim, A.B. Kozyrev, S.-J. Ho, D.W. van der Weide, *Microwave Symp. Dig. P.* **4** (2005)
60. H. Kim, S.-J. Ho, M.K. Choi, A.B. Kozyrev, D.W. van der Weide, *IEEE Trans. MTT* **54**, 4178 (2006)
61. H. Kim, A.B. Kozyrev, D.W. van der Weide, *IEEE Trans. MTT*, **55**, 571 (2007)
62. C. Qin, A.B. Kozyrev, A. Karbassi, D.W. van der Weide, *Metamaterials* **2**, 26 (2008)
63. N. Engheta, A. Salandrino, A. Alu, *Phys. Rev. Lett.* **95**, 95504 (2005)